



# Dynamic thermal diffusivity in three coexisting phases during phase transition of 4'-*n*-pentyloxybiphenyl-4-carbonitrile (5OCB)

Hidehiko Honda<sup>1</sup> · Hiroshi Ogura<sup>1</sup> · Hirokazu Kobayashi<sup>1</sup> · Yoshinobu Hosoi<sup>2</sup> · Masato Yamamoto<sup>1</sup>

Received: 27 October 2023 / Accepted: 29 May 2024  
© Akadémiai Kiadó, Budapest, Hungary 2024

## Abstract

When phase changes occur at slightly different times, the exothermic and endothermic phenomena cancel each other out in conventional thermal measurement methods, such as differential scanning calorimetry (DSC) and differential thermal analysis (DTA), making it challenging to capture them as changes in the DSC or DTA curves. We developed a new relaxation function to express the dynamic thermal diffusivity measured by alternating current (AC) calorimetry. This function helps analyze the frequency dependence of the endothermic or exothermic phenomena associated with phase transitions between phases that co-exist in a three-phase state. The new relaxation function was applied to analyze the phase transition phenomena that arise when 4'-*n*-pentyloxybiphenyl-4-carbonitrile (5OCB) is heated from the crystalline to the liquid-crystalline state. These phase transitions were investigated using DSC, polarization microscopy, and AC calorimetry. When microcrystals of 5OCB were heated at a rate of 15 °C h<sup>-1</sup> or less, three phases (two crystalline phases and a liquid-crystalline phase) were discovered to co-exist, and the endothermic (a phase transition from the crystalline to the liquid-crystalline phase) and exothermic (recrystallization) phenomena occurred in the same temperature range. Based on the different extent to which these phenomena depend on the frequency, a new relaxation function that considers the two relaxation processes was used to evaluate the frequency dependence of these phenomena. The respective relaxation times at 48.6 °C were 3.7 s (liquid crystallization) and 5.6 s (recrystallization).

**Keywords** Dynamic thermal diffusivity · Phase transition · Phase coexistence · Liquid-crystalline state · AC calorimetry · 4'-*n*-Pentyloxybiphenyl-4-carbonitrile (5OCB)

## Introduction

Thermodynamically, a phase transition phenomenon is considered to occur at a single point on a phase diagram. That is, the system is considered in the equilibrium state only before and after the phase transition; the non-equilibrium state during the phase transition is not considered. However, a sample that undergoes a phase transition due to a temperature change essentially has a nonuniform temperature distribution. This is because heat is transferred by way of conduction or convection within the sample, and

states in which phases co-exist arise within the sample owing to the nonuniformity of the temperature. Surface melting, surface crystallization, and structural changes during annealing occur under non-equilibrium conditions. Recently, as computing power has improved, the surface melting of ice has been reevaluated using computer simulations [1–3]. The presence of a quasi-liquid layer on the ice surface is thought to influence the shape of the snow and reduce the frictional force on the ice surface [4–6]. In addition, partial melting and liquid crystallization are widely observed in samples comprising molecules with many degrees of freedom, such as polymers and liquid crystal molecules, and even in hydrocarbon molecules with a degree of polymerization of approximately 30 [7–13]. These non-equilibrium states that appear during the changes associated with the phase transition phenomena depend on the rate at which the temperature increases or decreases, the crystallinity of the sample, and other factors. As phase transitions invariably pass through

✉ Hidehiko Honda  
hhonda@cas.showa-u.ac.jp

<sup>1</sup> Faculty of Arts and Sciences at Fujiyoshida,  
Showa University, 4562, Kamiyoshida,  
Fujiyoshida-shi, Yamanashi 403-0005, Japan

<sup>2</sup> Thermal Analysis Division, Rigaku Corporation, 3-9-12,  
Matsubara-cho, Akishima-shi, Tokyo 196-8666, Japan

non-equilibrium states, an analysis of the characteristics of these non-equilibrium states is essential for understanding the phase transitions [14, 15].

Among these non-equilibrium states, we investigated which two phases co-exist [9, 10]. Using alternating current (AC) calorimetry and microscopy, we studied the structural fluctuations at the interface between the two phases during phase transitions resulting from a slight temperature modulation by employing the relaxation time and relaxation strength of the dynamic thermal diffusivity. However, non-equilibrium states cannot be interpreted solely as fluctuations at the boundary of the two phases. These are the states in which the three phases co-exist. In a sample whose crystalline structure has been frozen before reaching the most thermodynamically stable state, such as the glassy state, phenomena that involve an increase in the molecular mobility upon heating (melting and a phase transition from the crystalline to the liquid crystal phase) and the phase transition to the most stable state due to increased mobility (recrystallization) may be observed in the same temperature range [16, 17]. In this case, three phases co-exist in the sample: a pre-melted crystalline phase, a liquid phase, and an energetically stable crystalline phase. Melting and recrystallization are endothermic and exothermic phenomena, respectively. Therefore, when these processes occur at slightly different times, the exothermic and endothermic phenomena cancel each other out in conventional thermal measurement methods, such as differential scanning calorimetry (DSC) and differential thermal analysis (DTA), making it difficult to capture them as changes in the DSC or DTA curves. Even for such phenomena, AC calorimetry can theoretically separate endothermic and exothermic reactions based on the differences in their frequency dependence; however, an analytical method to distinguish these phenomena has not yet been reported [18–24]. This led us to propose a new analytical method for the non-equilibrium state associated with a transition in which three phases co-exist; moreover, we propose a new relaxation equation for the dynamic thermal diffusivity. We also present the relaxation time and relaxation intensity of dynamic thermal diffusivity using 4'-*n*-pentyloxybiphenyl-4-carbonitrile (5OCB) as an example.

The properties of liquid crystals are often studied using 5OCB as a typical nematic liquid crystal [25–29]. 5OCB has attracted significant attention for technical applications because it has a liquid crystal state at 70 °C or lower and has high chemical stability [30–32]. Many studies have examined the properties of liquid crystals and their phase transition from the liquid crystal phase to the liquid phase; however, only a few focused on studying the phase transition from the crystal phase to the liquid crystal phase. In this study, we investigated the non-equilibrium state that arises during the phase transition from the crystalline to the liquid-crystalline phase in 5OCB using a new relaxation function.

## Experimental

### Cell assembly

A sample of 5OCB (99% pure) was acquired from Sigma-Aldrich Co., LLC. The sample was dissolved in ethanol and placed inside a sample cell for AC calorimetry measurement. The ethanol was volatilized using the concentration method, and the sample was recrystallized. The sample cell was cylindrical, as shown in Fig. 1. The bottom of the cell consisted of a cover glass, and the side surfaces were made of aluminum foil. The cover glass was ultrasonically cleaned for 1 h in distilled water and then immersed in acetone for 1 h. The surface of the cover glass was not subjected to any physical rubbing. The contact point of the alumel–chromel thermocouple was placed inside the cell. The diameter of the thermocouple wires was 0.1 mm.

### Differential scanning calorimetry (DSC)

The samples consisted of small crystals obtained by lightly crushing the crystals that formed in the sample cell for AC calorimetry. The mass of each sample was 6.0 mg. The sample pan and lid were fabricated from aluminum. The DSC curves were recorded using a DSC8240D instrument (Rigaku Co., Ltd.) with air as the surrounding atmosphere. The heating rates used were 5 °C h<sup>-1</sup>, 15 °C h<sup>-1</sup>, 120 °C h<sup>-1</sup>, and 240 °C h<sup>-1</sup>.

### Polarized microscopy

The samples observed with a polarized microscope were collected at the same time as the samples for DSC measurements. Thin plate-shaped microcrystals obtained when the crystals were crushed were used as the sample for observation. A sample cell with the same shape

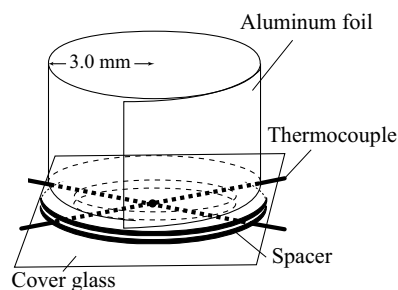


**Fig. 1** Cylindrical sample cell (radius: 3.0 mm; height: 10 mm). The bottom and sidewall of the cell comprised a cover glass and aluminum foil, respectively, and a PET sheet was used as the spacer. The sample temperature was measured with an alumel–chromel thermocouple

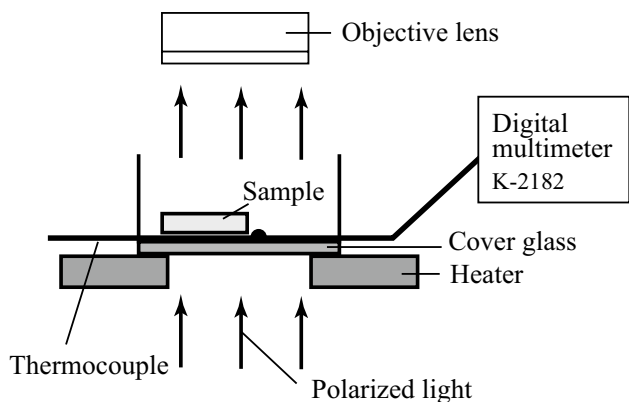


**Fig. 2** Temperature control attachment and sample cell for microscope. The cell was the same as shown in Fig. 1 but without the spacer between the glass and the thermocouple. To observe the sample with the polarizing microscope, the heater is arranged around the periphery of the cell to enable observation through the center

as depicted in Fig. 1 was placed on a heater and heated at a constant rate. Figure 2 shows the sample cell and the temperature controller attachment. The current flowing through the heaters was controlled using a stabilized DC power supply GPD-4303S (Good Will Instrument Co., Ltd.). The heating rate was maintained at  $15\text{ }^\circ\text{C h}^{-1}$ . An alumel–chromel thermocouple was placed in contact with the glass at the bottom of the cell, and the electromotive force was measured using a digital multimeter K2182 (TEXTRONIX, Inc.). The sample cell and the attachment were placed on the observation stage of a polarized microscope (LABOPHOT-POL, Nikon Imaging Japan Inc.) to observe the light passing through the sample.

### AC calorimetry

Heaters were installed around the sample cell to heat the sample at a rate of  $0.2\text{ }^\circ\text{C h}^{-1}$ , as shown in Fig. 3. The sample temperature was modulated by periodic irradiation with light from a halogen lamp. The light from the halogen lamp was periodically blocked by an electromagnetic shutter; hence, a rectangular heat flux pulse was supplied to the bottom surface of the sample. The glass at the bottom of the sample cell was painted black to improve light absorption. The reference frequencies of the heat flux pulses were set to 0.10 Hz, 0.05 Hz, and 0.02 Hz. The electromotive force of the thermocouple embedded in the sample was measured using a digital multimeter K2001 (TEXTRONIX, Inc.).

The AC heat flow supplied by the halogen lamp passed through the bottom glass and was conducted from the bottom to the top surface. Therefore, the AC component of the sample temperature,  $T_{ac}$ , is expressed by the following two one-dimensional heat conduction equations:

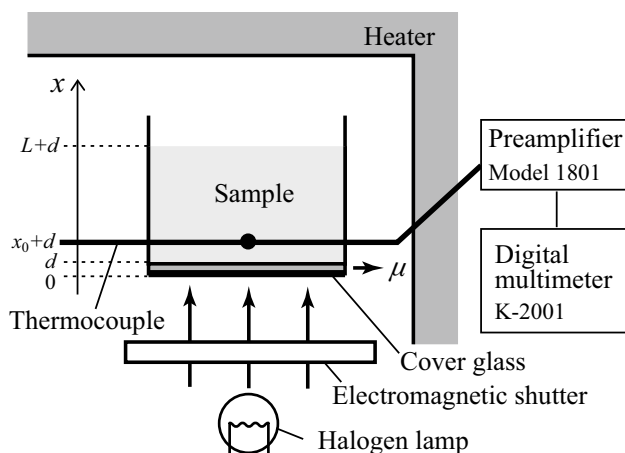


**Fig. 3** AC calorimeter. The temperature of the sample was modulated by using a halogen lamp to irradiate the bottom of the sample cell. The thickness of the bottom glass:  $d$ ; thickness of the sample:  $L$ ; distance from the top of the glass to the thermocouple:  $x_0$

$$\frac{\partial T_{ac}(x, t)}{\partial t} = a_g \frac{\partial^2 T_{ac}(x, t)}{\partial x^2} - \frac{Q(x, t)}{\rho_g c_g} \quad (0 \leq x \leq d) \quad (1)$$

$$\frac{\partial T_{ac}(x, t)}{\partial t} = a \frac{\partial^2 T_{ac}(x, t)}{\partial x^2} \quad (d \leq x \leq L + d) \quad (2)$$

where  $a_g$ ,  $\rho_g$ ,  $c_g$ , and  $d$  are the thermal diffusivity, density, specific heat, and glass thickness, respectively.  $a$  is the thermal diffusivity of the sample, and  $L$  is its thickness. The sample cell was placed in contact with the air at  $x = 0$ . The heat released to the outside via the glass surface, defined as  $Q(x, t)$ , is approximated as

$$Q(x, t) = \mu T_{ac}(x, t), \quad (3)$$

where  $\mu$  is a proportionality coefficient. The heat flux pulse input from the bottom is represented as

$$\dot{q}(0, t) = \frac{4\dot{q}_0}{\pi} \text{Im} \left( \sum_{m=0}^{\infty} \frac{\exp(i\omega_m t)}{2m + 1} \right) \quad m = 0, 1, 2, \quad (4)$$

Therefore,

$$T_{ac}(x_0 + d, t) = \frac{4\dot{q}_0}{\pi} \text{Im} \left\{ \sum_{m=0}^{\infty} \left( -\varepsilon \frac{\delta}{\gamma} + \sigma \right) \frac{\exp(i\omega_m t)}{2m + 1} \right\} \quad m = 0, 1, 2, \dots \quad (5)$$

$$\omega_m = (2m + 1)\omega_0 \quad m = 0, 1, 2, \dots \quad (6)$$

are obtained by solving Eqs. (1)–(3), where  $\omega_0$  is the angular frequency of the reference vibration component of the heat flux pulse,

$$\varepsilon = A(x_0)A'(d) + B(x_0)C'(d) \quad (7)$$

$$\delta = B'(d)\{A(L) - RC(L)\} + A'(d)\{B(L) - RA(L)\} \quad (8)$$

$$\gamma = A'(d)\{A(L) - RC(L)\} + C'(d)\{B(L) - RA(L)\} \quad (9)$$

$$\sigma = A(x_0)B'(d) + B(x_0)A'(d) \quad (10)$$

and, then

$$A(x) = \cos h k x \quad (11)$$

$$B(x) = \frac{-\sin h k x}{\kappa k} \quad (12)$$

$$C(x) = -\kappa k \sin h k x \quad (13)$$

$$k = \sqrt{\frac{i\omega}{a}} \quad (14)$$

$$A'(x) = \cosh k' x \quad (15)$$

$$B'(x) = \frac{-\sinh k' x}{\kappa k'} \quad (16)$$

$$C'(x) = -\kappa k' \sinh k' x \quad (17)$$

$$k' = \sqrt{\frac{i\omega\rho_g c_g + \mu}{\kappa_g}} \quad (18)$$

Here,  $\kappa$  and  $\kappa_g$  are the thermal conductivity of the sample and that of the glass, respectively.

## Results

### DSC measurement and microscope observation

Figure 4 shows the dependence of the DSC curves on the heating rate. Endothermic peaks were detected at approximately 50 °C (peak A) and approximately 69 °C (peak C) regardless of the heating rate. In addition, the roughness of the DSC curve was measured at a temperature lower than peak A in the temperature range  $\beta_1$ . The appearance of peak B, measured in the temperature range  $\beta_3$ , depended on the heating rate and appeared for heating rates of 15 °C h<sup>-1</sup> or

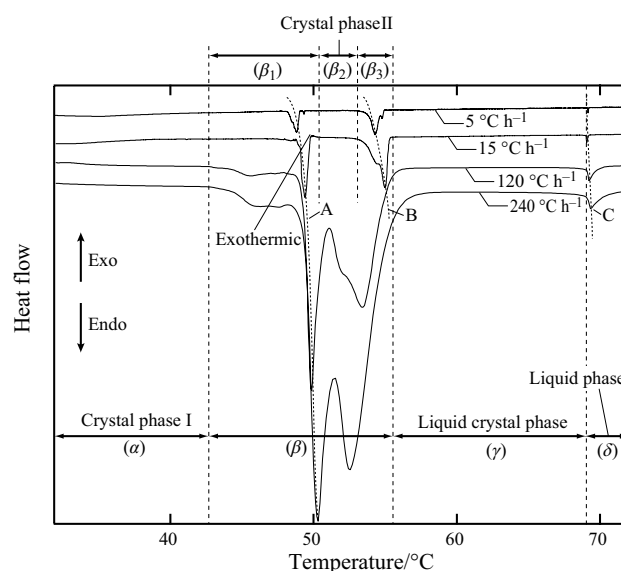


**Fig. 4** Dependence of DSC curve on heating rate. The four curves are vertically offset and aligned in the order of increasing heating rate 5 °C h<sup>-1</sup>, 15 °C h<sup>-1</sup>, 120 °C h<sup>-1</sup>, and 240 °C h<sup>-1</sup>. The endothermic peaks near 50 °C and 69 °C are designated peaks A and C, respectively. Peak C represents an endotherm associated with a phase transition from the liquid crystal phase to the liquid phase. Temperature range  $\alpha$ : up to 43 °C;  $\beta$ : from 43 to 56 °C;  $\gamma$ : from 56 to 69 °C;  $\delta$ : from 69 °C. An endothermic peak B appeared for curves with heating rates of 5 °C h<sup>-1</sup> and 15 °C h<sup>-1</sup>. Temperature range  $\beta$ :  $\beta_1$  up to 51 °C;  $\beta_2$ : from 51 to 53 °C;  $\beta_3$ : from 53 °C and higher. An exothermic peak is seen on the high-temperature side of peak A in the DSC curve at a heating rate of 15 °C h<sup>-1</sup>

less. A small exothermic peak was observed on the high-temperature side of  $\beta_1$  for the heating rate of 15 °C h<sup>-1</sup>.

Figure 5 shows the photographic images acquired using the polarizing microscope. Figure 5a presents the crystal phase observed at 32 °C, denoted as phase I. Figure 5b shows an image captured at 49 °C after the sample was heated at a rate of 15 °C h<sup>-1</sup>. During this time, the crystal surface transitioned to the liquid crystal phase, which was characterized by the appearance of needle-like crystals. The recrystallized phase, denoted as phase II, transitioned to the liquid crystal phase at approximately 55 °C. When the phase transition from the crystalline to the liquid-crystalline phase was observed using a polarizing microscope, it was evident that the outer periphery of the crystal underwent deformation. Molecular fluidity is enhanced in the liquid crystal phase compared to the crystalline phase; however, the short-range order of molecular orientation is maintained. Even in substances such as paraffin that do not exhibit a liquid crystal state, the outer periphery of the crystal undergoes shape changes upon melting. However, there is a notable difference in the birefringence index between the liquid crystal and liquid phase states. The liquid phase portion appears transparent under polarizing microscopy because the birefringence

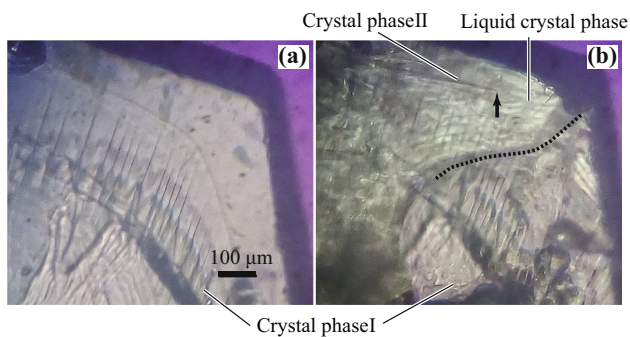


**Fig. 5** Polarizing microscope images captured at 32 °C (a) and 49 °C (b) after heating the sample at a rate of 15 °C h<sup>-1</sup>. The liquid crystal phase grew from the left to the right at 49 °C. The dotted curve in (b) shows part of the boundary at the interface between the liquid-crystalline and crystalline phases. Recrystallization proceeded from the left to the right in the liquid crystal phase. The crystal phase generated by recrystallization is called crystal phase II, which exhibited needle-like crystals. The arrow in the figure indicates the tip of a needle

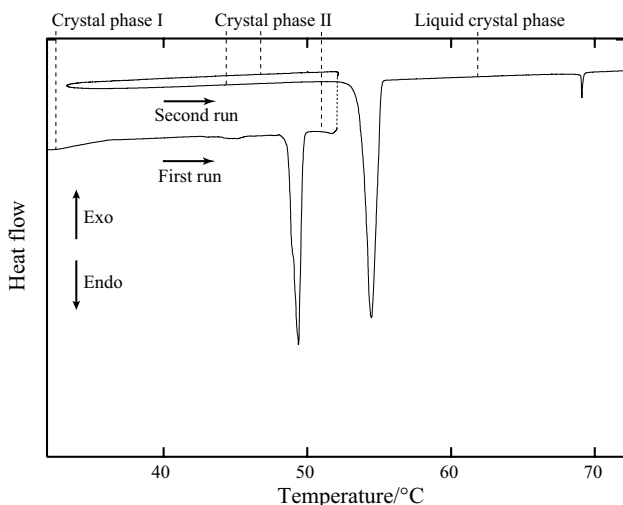


**Fig. 6** DSC curves. Both the heating and cooling rates were 15 °C h<sup>-1</sup>. The temperature was lowered to 33 °C after heating to 52 °C, then increased again. The DSC curve (shown as a solid line) was measured as a continuous curve but is cut off at 52 °C, and the display is shifted in the vertical direction for ease of viewing

index is zero. Conversely, the liquid crystal phase part is opaque due to the birefringence phenomenon that depends on molecular orientation. The color of the crystal surface area that undergoes a phase transition to the liquid crystal phase in Fig. 5b changes because an opaque liquid crystal layer covers the surface.

The DSC curve was recorded while the sample was heated to 52 °C, cooled to 33 °C, and then reheated to 72 °C. The DSC curves are shown in Fig. 6. The heating and cooling rates were maintained at 15 °C h<sup>-1</sup>. An endothermic peak was observed at 49 °C during the first heating step to 52 °C. Based

on the images captured using the microscope, this abnormality in the specific heat represented an endothermic reaction accompanying the phase transition from phase I to phase II through the liquid crystal phase. Subsequently, no exothermic peak was observed even when the temperature was lowered to 33 °C. This indicated that the state of the sample did not return to phase I. Renewed heating gave rise to an endothermic peak at 53 °C, which indicated that an endothermic phenomenon accompanied the transition to the liquid crystal phase. Considering that the endothermic reaction corresponding to peak A did not occur during reheating, this led to the conclusion that phases I and II were different. Figure 7 shows images of the crystals observed using the polarizing microscope with a heating rate of 120 °C h<sup>-1</sup>. Owing to the rapid heating rate, the liquid crystal phase rapidly formed at 50 °C; all the crystals transitioned to the liquid crystal phase. In this case, phase II does not occur in the crystals.

### AC calorimetry

AC calorimetry measurements were performed in the temperature range  $\beta_1$ . The measurement was also performed at 33.4 °C, where no phase transition occurs. Figure 8 shows the temperature waveforms, with Fig. 8a showing the waveform measured at 33.4 °C. The waveform was triangular because the AC heat pulse supplied by the halogen lamp was conducted through the sample. The shape of the waveform changes in the temperature range of the phase transition. Figure 8b represents the temperature waveform measured at 48.6 °C. This temperature is close to the temperature at which peak A appears on the DSC curve. The rate of temperature increase in period II of the waveform shown in Fig. 8b is lower than that shown in Fig. 8a. In Fig. 8b, the change in the rate at which the temperature decreased during the cooling period between time ranges I,' II,' and III' was also measured.

## Discussion

### Surface liquid crystallization and recrystallization

The polarizing microscopy results (Fig. 5) indicated that during heating, phase I did not undergo a direct transition to phase II; instead, the transition proceeded via the liquid crystal phase at the surface. Peak A in Fig. 4 represents an endotherm resulting from the phase transition from phase I to the liquid crystal phase. Further, the exothermic peak measured at the 15 °C h<sup>-1</sup> heating rate indicates recrystallization from the liquid crystal phase to phase II.



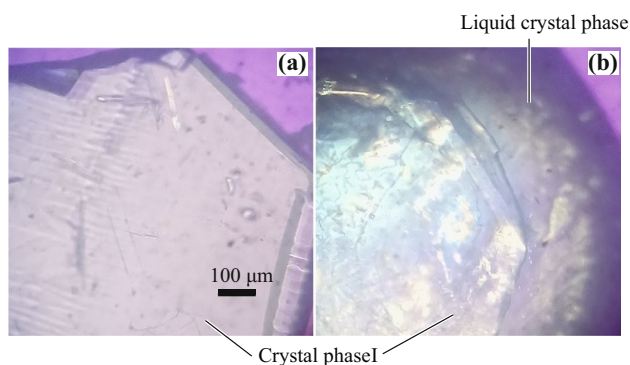


**Fig. 7** Optical images captured using the polarizing microscope at 32 °C (a) and 50 °C (b). The heating rate was 120 °C h<sup>-1</sup>. The phase transition from the crystalline to the liquid-crystalline phase started on the surface of the crystal, after which the entire region transitioned to the liquid-crystalline phase without recrystallization to phase II at 50 °C

### Crystal nucleation and phase coexistence

As shown in Fig. 7, recrystallization of the liquid crystal phase to phase II progressed slowly, and, at high heating rates, the crystal nuclei disappeared before recrystallization. The transition to phase II was undetected in the sample region, where the crystal nuclei disappeared and fully transitioned to the liquid crystal towards the high-temperature side of the temperature range  $\beta$  for high heating rates.

In the measurements shown in Fig. 6, the endothermic reaction corresponding to peak A did not occur when the temperature increased again. Therefore, it can be concluded that phase I did not form in the temperature range  $\beta_2$ . In addition, no exothermic phenomena were observed

when the temperature decreased. Thus, it was not easy to generate the nuclei of phase I in the sample region where the transition to phase II was complete.

The above results show that the sample in the temperature range  $\beta_1$  was in the state in which the three phases of the crystal, namely, phase I, phase II, and the liquid crystal phase, co-existed, and in the temperature range  $\beta_2$ , the sample was in phase II.

### Measurement of relaxation time of phase transition

In Fig. 8b, the rate at which the temperature increases decreases from region I to region II. This rate change could be attributed to an endothermic reaction that accompanied the phase transition; similar behavior has been reported for many phase transition phenomena. This decrease in the rate of temperature increase can be explained by expanding the specific heat to dynamic specific heat, which is a complex specific heat with frequency dependence [18–21]. The simplest frequency dependence of dynamic specific heat can be expressed using the Debye relaxation function. The real part  $C'$  and the imaginary part  $C''$  of the dynamic specific heat were set as follows:

$$C' = C_{\infty} + \frac{\Delta C_1}{1 + \omega^2 \tau_1^2} \quad (19)$$

$$C'' = \frac{\Delta C_1 \omega \tau_1}{1 + \omega^2 \tau_1^2}, \quad (20)$$

where  $C_{\infty}$  is the specific heat of the high-frequency limit,  $\Delta C_1$  is the relaxation strength,  $\omega$  is the angular frequency, and  $\tau_1$  is the relaxation time. In this study, the specific heat could not be determined independently; however, the thermal diffusivity could be obtained. Assuming that the frequency dependences of the density and thermal conductivity are negligible, the Debye relaxation can be represented as

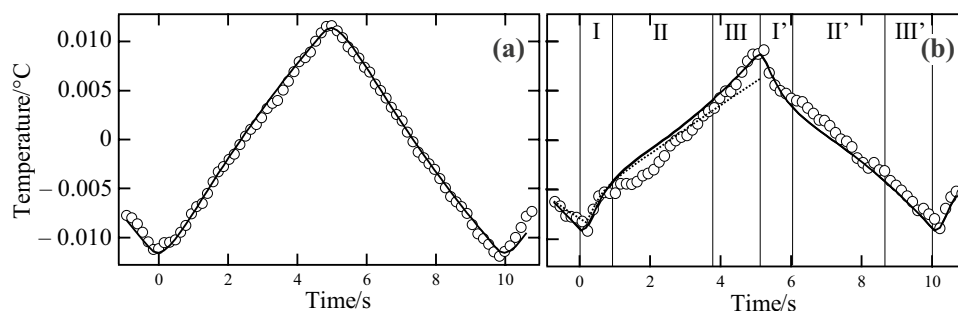


**Fig. 8** AC calorimetry temperature waveforms measured at 33.4 °C (a) and 48.6 °C (b). Open circles: measured data; solid lines: fitted curves. The dotted line is calculated using Eqs. (21) and (22). The reference frequency of the AC heat flux was 0.10 Hz. Irradiation of the sample cell with the halogen lamp: 0 s to 5 s (heating); irradiation

discontinued by closing the electromagnetic shutter: 5 s to 10 s (cooling). The heating and cooling periods are divided into three periods: I, II, III, and I', II', and III', respectively. Each change in the curvature of the temperature waveform forms the boundary of a time period

$$A' = \left(\frac{1}{a^*}\right)' = A_\infty + \frac{\Delta A_1}{1 + \omega^2 \tau_1^2} \quad (21)$$

$$A'' = \left(\frac{1}{a^*}\right)'' = \frac{\Delta A_1 \omega \tau_1}{1 + \omega^2 \tau_1^2} \quad (22)$$

by expressing the inverse of the dynamic thermal diffusivity  $1/a^*$  by  $A$ . The fitting curve calculated by substituting the relaxation Eqs. (21), (22) into Eq. (14) is represented by the dotted line in Fig. 8b. This curve could explain the curvature change from period I to period II but not the curvature change from period II to period III. Therefore, the following new relaxation formula was generated assuming double relaxation, where  $\Delta A_2$  and  $\tau_2$  are the newly introduced relaxation strength and relaxation time, respectively.

$$A' = \left(\frac{1}{a^*}\right)' = A_\infty + \frac{\Delta A_1}{1 + \omega^2 \tau_1^2} + \frac{\Delta A_2}{1 + \omega^2 \tau_2^2} \quad (23)$$

$$A'' = \left(\frac{1}{a^*}\right)'' = \frac{\Delta A_1 \omega \tau_1}{1 + \omega^2 \tau_1^2} + \frac{\Delta A_2 \omega \tau_2}{1 + \omega^2 \tau_2^2}, \quad (24)$$

The curve plotted using Eqs. (23), (24) is represented by the solid line in Fig. 8b and was fitted to the measured values. The real part  $A'$  and imaginary part  $A''$  of  $A$  were obtained by fitting the calculated curves to the results measured at the reference frequencies of 0.10 Hz, 0.05 Hz, and 0.02 Hz. Figure 9 shows the frequency dependence of  $A$ . In addition to the reference frequency component of  $A$  ( $\omega_0$  in Eq. (6), that is, 0.10 Hz, 0.05 Hz, and 0.02 Hz), the values of the third-order vibration component ( $m=1$ ) and the fifth-order vibration component ( $m=2$ ) are also shown. Figure 10 shows the temperature dependence of the relaxation parameters obtained from the fitting curves of  $A'$  and  $A''$ . The relaxation strength  $\Delta A_2$  was zero at 43.4 °C and below. This indicates that the waveform can be fitted using the relaxation Eqs. (21) and (22). Conversely, the relaxation strength  $\Delta A_2$  at 43.6 °C and higher was negative, and the relaxation time  $\tau_2$  was larger than  $\tau_1$  at 44.2 °C and above.

### Relaxation parameters of the heating process (periods I, II, and III)

The second term of the real part  $A'$  in Eq. (23),

$$\frac{\Delta A_2}{1 + \omega^2 \tau_2^2},$$

and the first term of the imaginary part  $A''$  in Eq. (24),

$$\frac{\Delta A_2 \omega \tau_2}{1 + \omega^2 \tau_2^2},$$

represents the change in thermal diffusivity because of the endotherm accompanying the phase transition in periods I, II, and III. The third term in the real part  $A'$ ,

$$\frac{\Delta A_2}{1 + \omega^2 \tau_2^2},$$

and the second term in the imaginary part  $A''$ ,

$$\frac{\Delta A_2 \omega \tau_2}{1 + \omega^2 \tau_2^2},$$

are considered to represent the exothermic phenomenon, assuming that  $\Delta A_2$  was negative. The DSC measurements and observations with the microscope showed that the sample surface transitioned from phase I to the liquid crystal phase during heating, which was an endothermic phenomenon. Subsequently, recrystallization to phase II was observed in the liquid crystal phase, which was an exothermic phenomenon. Therefore,  $\Delta A_1$  and  $\tau_1$  are considered to represent the relaxation strength and relaxation time in the relaxation phenomenon of the phase transition from phase I to the liquid crystal phase, and  $\Delta A_2$  and  $\tau_2$  those of the recrystallization from the liquid crystal phase to phase II. This phase transition is indicated by the solid arrow in Fig. 11. In the liquid crystal phase, the molecules are highly fluid, and they readily take on different arrangements. In addition, because the molecules are more ordered than those in the liquid phase, little activation energy is required to convert the liquid crystal phase to phase I.

### Relaxation phenomenon of the cooling process (periods I', II'', and III''')

The temperature was periodically modulated using AC calorimetry, which, as shown in Fig. 8, enabled the temperature

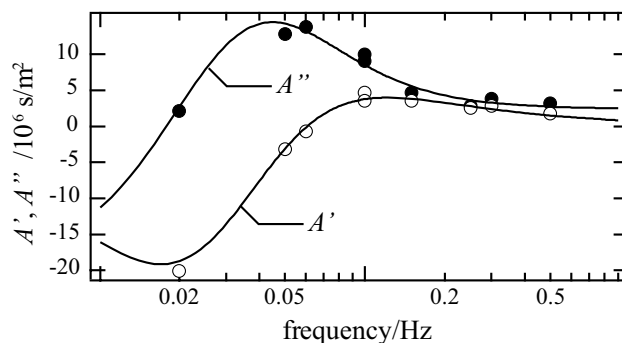


**Fig. 9** Frequency dependence of  $A$ .  $A$  represents  $1/a^*$ , where  $a^*$  is the dynamic thermal diffusivity.  $A'$  and  $A''$  are the real and imaginary parts of  $A$ , respectively. Open and solid circles represent data obtained from the temperature waveform at 48.6 °C, and the solid curves represent fitted data

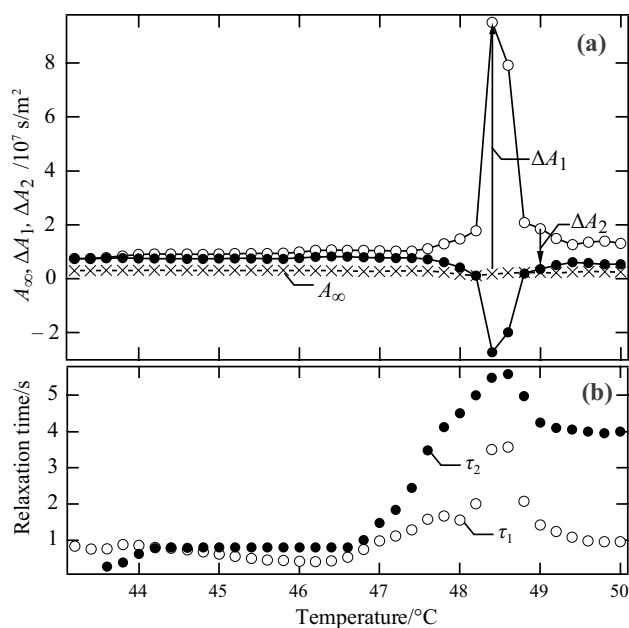


**Fig. 10** Temperature dependence of the relaxation parameters  $A_\infty$ ,  $\Delta A_1$ , and  $\Delta A_2$  (a);  $\tau_1$  and  $\tau_2$  (b). Crosses ( $\times$ ) indicate  $A_\infty$ . The difference between  $\times$  and  $\circ$  represents  $\Delta A_1$ , and the difference between  $\circ$  and  $\bullet$  represents  $\Delta A_2$ . Because  $\bullet$  is smaller than  $\circ$ ,  $\Delta A_2$  is negative. The respective relaxation times at 48.6 °C were 3.7 s (liquid crystallization) and 5.6 s (recrystallization)

to be lowered in 5 s (from 5 to 10 s) in the case of 0.10 Hz. As shown in Fig. 8b, the change in the temperature waveform curvature was symmetric during the heating (from 0 to 5 s) and cooling (from 5 to 10 s) processes. This indicates that during the cooling process, an endothermic phenomenon occurred after the exothermic phenomenon and that the relaxation parameters were sufficiently close to those in the heating process. The phase transition during the cooling process is presumably indicated by the dotted arrow in Fig. 11. The transition from the liquid crystal phase to phase I is an exothermic reaction, whereas the transition from phase I to phase II is endothermic. The change in energy owing to the phase transition, indicated by the dotted arrow, is not the same as that indicated by the solid arrow. However, the difference between the relaxation parameters of the heating and cooling processes is considered negligible because of the small amplitude of the temperature modulated by the AC calorimetry; the large sample size caused the inhomogeneity in the sample.

Figure 12 shows a schematic of the phase transition where all three phases of the crystal, that is, phase I, phase II, and the liquid crystal phase, co-exist. The phase transition between phase I and the liquid crystal phase readily occurs, and the relaxation time is short. In contrast, the phase transition from phase I or from the liquid-crystal phase to phase

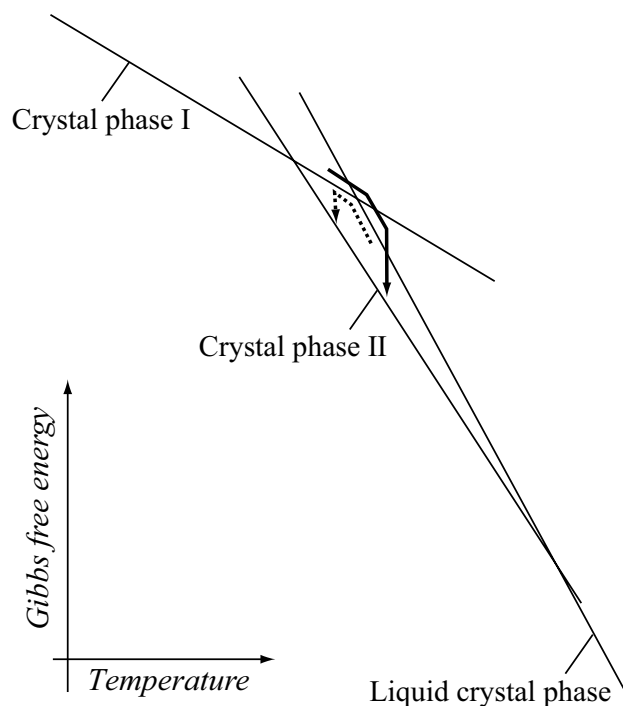


**Fig. 11** Temperature dependence of Gibbs energy. Solid arrow: crystal phase I transitions to liquid crystal phase and crystal phase II (heating process). Dotted arrow: liquid crystal phase transitions to phase I and then to phase II (cooling process)

II is considered a relaxation phenomenon with a relatively long relaxation time.

### Relaxation strength and relaxation time

The relaxation phenomenon represented by the Debye-type relaxation equation shows a simple time variation that changes exponentially from one equilibrium state to another. The relaxation time indicates the speed of change and corresponds to the magnitude of activation energy. The relaxation strength corresponds to the magnitude of heat absorption and exothermal activity. In the experiments with 50CB as the sample, the relaxation time and strength showed a temperature dependence with a peak between 48.5 °C and 48.6 °C. At temperatures lower than the peak, both the relaxation strength and relaxation time were small, suggesting that the phase transition was mainly a microscopic phase transition on the surface of crystalline phase I. At the high-temperature side, including the peak, it is hypothesized that a phase transition with relatively high activation energy occurs, which is related to the growth of the needle-like crystalline phase II, as shown in Fig. 5b.

The relaxation Eqs. (23), (24) proposed in this study are a combination of Debye-type relaxations and are highly versatile. These equations apply to phase transitions in



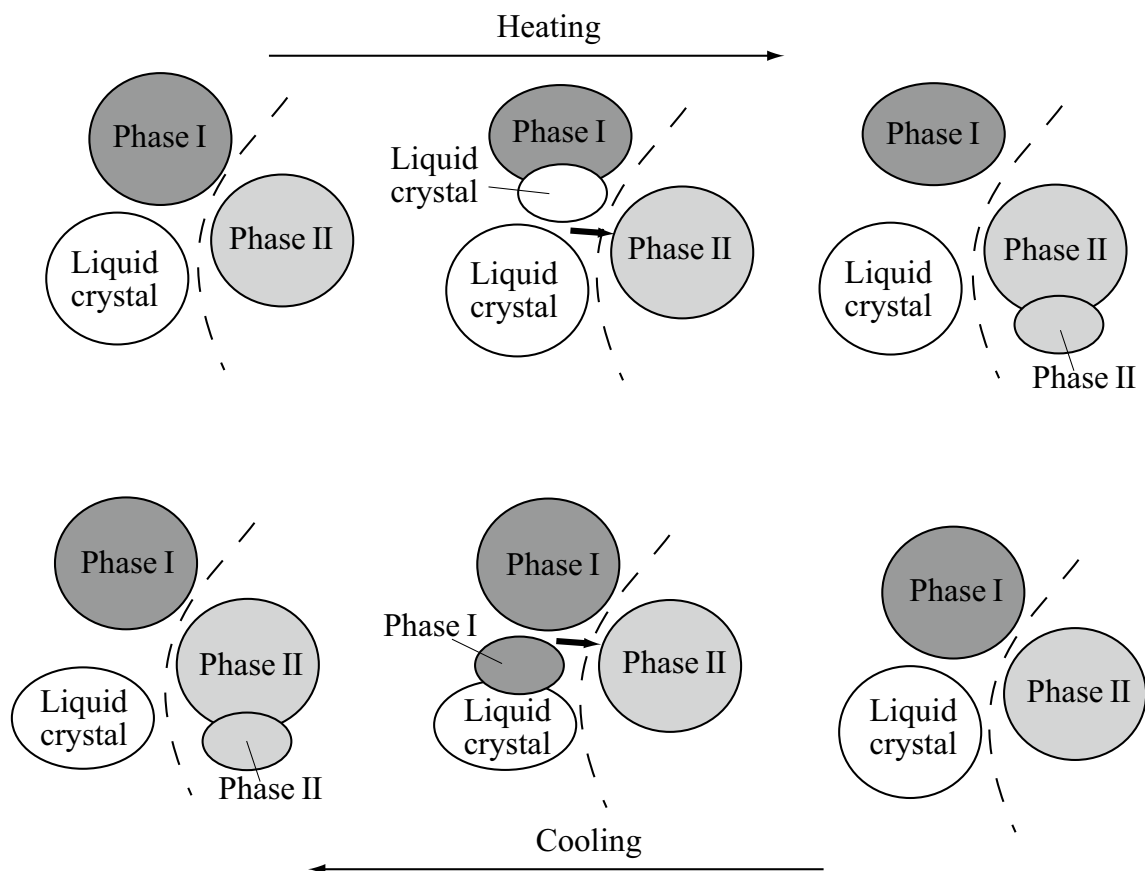


**Fig. 12** Schematic diagram of the phase transition. Three phases co-exist through the phase transition: crystal phase I, crystal phase II, and the liquid crystal phase. The heating and cooling processes cor-

respond to the processes indicated by the solid and dotted arrows in Fig. 11, respectively

which two relaxation phenomena with different relaxation times occur simultaneously. Even in the case of surface melting of water, a molecule widely studied, the mechanism of surface melting and accompanying recrystallization remains unclear. We anticipate that the analysis method proposed in this study will contribute to the clarification of non-equilibrium states, such as surface melting, where multiple phases co-exist at the same temperature, and endothermic and exothermic phenomena occur simultaneously, not limited to 5OCB.

## Conclusions

We derived a relaxation function to express the dynamic thermal diffusivity in systems where two independent relaxation phenomena were observed as follows:

$$A' = A_{\infty} + \frac{\Delta A_1}{1 + \omega^2 \tau_1^2} + \frac{\Delta A_2}{1 + \omega^2 \tau_2^2}$$

$$A'' = \frac{\Delta A_1 \omega \tau_1}{1 + \omega^2 \tau_1^2} + \frac{\Delta A_2 \omega \tau_2}{1 + \omega^2 \tau_2^2},$$

where  $A'$  and  $A''$  are the real and imaginary parts of dynamic thermal diffusivity, respectively. This function was applied to the results obtained by AC calorimetry in the crystalline to liquid crystal phase transition temperature range of 5OCB. During the phase transition of 5OCB, three phases (crystalline phase I, crystalline phase II, and a liquid-crystalline phase) co-existed when measured at a heating rate of  $15 \text{ }^{\circ}\text{C h}^{-1}$  or less. Analysis using the above formula revealed that the relaxation strength of each phenomenon was positive ( $\Delta A_1$ ) and negative ( $\Delta A_2$ ). That is, it is possible to distinguish between the relaxation phenomenon (endothermic reaction) associated with the phase transition from crystal phase I to the liquid crystal phase and that (exothermic reaction) associated with the phase transition from the liquid crystal phase to crystal phase II by the sign of the relaxation strength. Furthermore, the relaxation time was determined using the relaxation function. The relaxation time was as long as 3.7 s for liquid crystallization and as much

as 5.6 s for recrystallization. As described above, in this paper, we proposed a new relaxation function and showed that applying this relaxation function to actual measurement results enables the frequency dependence of each relaxation phenomenon to be determined. In phase transitions where melting, liquid crystallization, and recrystallization occur in the same temperature range, it is difficult to estimate the endothermic and exothermic values of each phenomenon by conventional DSC and DTA because the endothermic and exothermic values of each phenomenon cancel each other out. However, if the frequency dependence of each phenomenon is different, the relaxation strength and relaxation time of each phenomenon can be evaluated independently using the relaxation functions proposed in this study.

**Acknowledgments** We thank Editage ([www.editage.com](http://www.editage.com)) for their English language-editing support.

## Declarations

**Conflict of interest** The authors have no conflicts of interest to declare relevant to this article's content.

## References

- Qiu Y, Molinero V. Why is it so difficult to identify the onset of ice premelting? *J Phys Chem Lett*. 2018. <https://doi.org/10.1021/acs.jpcclett.8b02244>.
- Sibley DN, Lombart P, Noya EG, Archer AJ, MacDowell LG. How ice grows from premelting films and water droplets. *Nat Commun*. 2021. <https://doi.org/10.1038/s41467-020-20318-6>.
- Slater B, Michaelides A. Surface premelting of water ice. *Nat Rev Chem*. 2019. <https://doi.org/10.1038/s41570-019-0080-8>.
- Bartels-Rausch T, Jacobi HW, Kahan TF, Thomas JL, Thomson ES, Abbott JPD, et al. A review of air–ice chemical and physical interactions (AICI): liquids, quasi-liquids, and solids in snow. 2014. *Atmos Chem Phys*. <https://doi.org/10.5194/acp-14-1587-2014>.
- Weber B, Nagata Y, Ketzetzi S, Tang F, Smit WJ, Bakker HJ, Backus EHG, Bonn M, Bonn D. Molecular insight into the slipperiness of ice. *J Phys Chem Lett*. 2018. <https://doi.org/10.1021/acs.jpcclett.8b01188>.
- Canale L, Comtet J, Niguès A, Cohen C, Clanet C, Siria A, Bocquet L. Nanorheology of interfacial water during ice gliding. *Phys Rev X*. 2019. <https://doi.org/10.1103/PhysRevX.9.041025>.
- Phuong-Nguyen H, Charlet G, Delmas G. Slow calorimetry and heat of fusion of poly(4-methyl pentene-1). *J Therm Anal*. 1996. <https://doi.org/10.1007/BF01983604>.
- Sirota EB. Supercooling, nucleation, rotator phases, and surface crystallization of n-alkane melts. *Langmuir*. 1998. <https://doi.org/10.1021/la970594s>.
- Honda H, Ogura H. Reversing and non-reversing melting of n-hexatriacontane: in situ optical observation study. *Thermochim Acta*. 2012. [https://doi.org/10.1016/S0040-6031\(03\)00135-7](https://doi.org/10.1016/S0040-6031(03)00135-7).
- Honda H. In situ temperature-modulated microscopy observation of two-phase co-existing states of coumarin and coumarin derivative in melting. *J Therm Anal Calorim*. 2019. <https://doi.org/10.1007/s10973-018-7952-x>.
- Xu J, Reiter G, Alamo RG. Concepts of nucleation in polymer crystallization. *Crystals*. 2021. <https://doi.org/10.3390/cryst11030304>.
- Sangroniz L, Wang B, Su Y, Liu G, Cavallo D, Wang D, et al. Fractionated crystallization in semicrystalline polymers. *Prog Polym Sci*. 2021. <https://doi.org/10.1016/j.progpolymsci.2021.101376>.
- Rozwadowski T, Yamamura Y, Saito K. Interplay between melt and cold crystallization in a smectic liquid crystal, 4-pentylphenyl 4-(trans-4-pentylcyclohexyl)benzoate. *Cryst Growth Des*. 2021. <https://doi.org/10.1021/acs.cgd.0c01682>.
- Bellantuono L, Janik RA, Jankowski J, Soltanpanahi H. Dynamics near a first order phase transition. *J High Energy Phys*. 2019. [https://doi.org/10.1007/JHEP10\(2019\)146](https://doi.org/10.1007/JHEP10(2019)146).
- Yan H, Zhang F, Wang J. Thermodynamic and dynamical predictions for bifurcations and non-equilibrium phase transitions. *Commun Phys*. 2023. <https://doi.org/10.1038/s42005-023-01210-3>.
- Teitelbaum BY. Some features of polymer crystallization and melting as exposed by DTA of poly(ethylene adipate). *J Therm Anal*. 1975;8:511. <https://doi.org/10.1007/BF01910130>.
- Ling X, Spruiell JE. Analysis of the complex thermal behavior of poly(L-lactic acid) film I. Samples crystallized from the glassy state. *J Polym Sci Part B: Polym Phys*. 2006. <https://doi.org/10.1002/polb.20972>.
- Albrecht T, Armbruster S, Keller S, Strobl G. Dynamics of surface crystallization and melting in polyethylene and poly(ethylene oxide) studied by temperature-modulated DSC and heat wave spectroscopy. *Macromolecules*. 2001. <https://doi.org/10.1021/ma0106595>.
- Schawe JEK, Hutter T, Heitz C, Alig I, Lellinger D. Stochastic temperature modulation: a new technique in temperature-modulated DSC. *Thermochim Acta*. 2006. <https://doi.org/10.1016/j.tca.2006.01.031>.
- Chua YZ, Zorn R, Holderer O, Schmelzer JWP, Schick C, Donth E. Temperature fluctuations and the thermodynamic determination of the cooperativity length in glass forming liquids. *J Chem Phys*. 2017. <https://doi.org/10.1063/1.4977737>.
- Alig I, Böhm F, Lellinger D. Heat capacity spectroscopy by using stochastic temperature modulated calorimetry: Time-temperature superposition and fictive temperature at the glass transition of poly(vinyl acetate). *Thermochim Acta*. 2019. <https://doi.org/10.1016/j.tca.2019.03.010>.
- Romero FJ, Gallardo MC, Martín-Olalla JM, del Cerro J. Experimental method to determine specific heat capacity and transition enthalpy at a first-order phase transition: Fundamentals and application to a Ni-Mn-In Heusler alloy. *Thermochim Acta*. 2021. <https://doi.org/10.1016/j.tca.2021.179053>.
- Garden JL, Peyrard M. Understanding temperature-modulated calorimetry through studies of a model system. *Phys Rev E*. 2022. <https://doi.org/10.1103/PhysRevE.105.034144>.
- Qiu L, Ouyang Y, Li F. Chapter 2 - Experimental techniques overview. In: Qiu L, Li F, editors. *Micro and nano thermal transport*. London: Academic Press; 2022. p. 19–45.
- de Groen M, Vlught TJH, de Loos TW. Phase behavior of liquid crystals with CO<sub>2</sub>. *J Phys Chem B*. 2012. <https://doi.org/10.1021/jp303426k>.
- de Groen M, Matsuda H, Vlught TJH, de Loos TW. Phase behaviour of the system 4'-pentyl-4-cyanobiphenyl + CO<sub>2</sub>. *J Chem Thermodyn*. 2013. <https://doi.org/10.1016/j.jct.2012.11.026>.
- Chen Z, Jiang Y, Jiang L, Ma H. Terahertz absorption spectra and potential energy distribution of liquid crystals. *Spectrochim Acta A*. 2016. <https://doi.org/10.1016/j.saa.2015.09.024>.
- Oweimreen GA, Morsy MA. DSC studies on p-(n-alkyl)-p'-cyanobiphenyl (RCB's) and p-(n-alkoxy)-p'-cyanobiphenyl (ROCB's) liquid crystals. *Thermochim Acta*. 2000. [https://doi.org/10.1016/S0040-6031\(99\)00411-6](https://doi.org/10.1016/S0040-6031(99)00411-6).

29. Ryu M, Batsale JC, Morikawa J. Quadrupole modelling of dual lock-in method for the simultaneous measurements of thermal diffusivity and thermal effusivity. *Int J Heat Mass Transf.* 2020. <https://doi.org/10.1016/j.ijheatmasstransfer.2020.120337>.
30. Williams VE, Robert PL. Role of dispersion and electrostatic forces on solute–solvent interactions in a nematic liquid crystal phase. *J Am Chem Soc.* 1998. <https://doi.org/10.1021/ja982727h>.
31. Ryu M, Takezoe H, Haba O, Yonetake K, Morikawa J. Photo-controllable thermal diffusivity and thermal conductivity driven by the orientation change of nematic liquid crystal with azo-dendrimers. *J Appl Phys Lett.* 2015. <https://doi.org/10.1063/14936374>.
32. Bielejewska N, Hertmanowski R. Functionalization of LC molecular films with nanocrystalline cellulose: a study of the

self-assembly processes and molecular stability. *Colloids Surf.* 2020. <https://doi.org/10.1016/j.colsurfb.2019.110634>.

**Publisher's Note** Springer Nature remains neutral with regard to jurisdictional claims in published maps and institutional affiliations.

Springer Nature or its licensor (e.g. a society or other partner) holds exclusive rights to this article under a publishing agreement with the author(s) or other rightsholder(s); author self-archiving of the accepted manuscript version of this article is solely governed by the terms of such publishing agreement and applicable law.